

Investigation of Water Evaporation and Salt Precipitation at CO₂ Geological Storage Condition

Zhe Wang¹, Panrui Yang¹, Huirong Guo¹, Qian Zhou¹, Linlin Lin², and Min Yuan¹

¹China University of Geosciences

²Shandong Provincial Lunan Geology and Exploration Institute (Shandong Provincial Bureau of Geology and Mineral Resources NO.2 Geological Brigade)

November 22, 2022

Abstract

CO₂ geological storage is a promising method to dispose excess CO₂ in the atmosphere, and the existence of brine in deep saline aquifer and below oil reservoir may lead to salt precipitation in pore space for dry-out formation. Water diffusion coefficient is helpful to evaluate salt precipitation. However, limited previous data cant satisfy the need of CO₂ geological storage. Raman quantitative spectroscopy is used to observe water diffusion in CO₂ in a high-pressure capillary cell and corresponding diffusion coefficients are obtained at 10-50 MPa and 353.15-433.15 K. Diffusion coefficient is temperature and pressure dependent, and also increases linearly with the reciprocal of CO₂ density. Free volume theory and PC-SAFT EOS are utilized to establish a thermodynamic model for water diffusion in CO₂, and it predicts diffusion coefficient accurately at 10-50 MPa and 353.15-433.15 K. Besides, diffusion coefficient is used to evaluate when salt precipitation occurs and salt precipitation process is observed in a one-dimensional capillary tube and a two-dimensional micromodel respectively.

1
2
3
4
5
6
7
8
9
10
11
12
13
14

Investigation of Water Evaporation and Salt Precipitation at CO₂ Geological Storage Condition

Zhe Wang¹, Panrui Yang¹, Huirong Guo^{1†}, Qian Zhou¹, Linlin Lin² and Min Yuan¹

¹School of Environmental Studies, China University of Geosciences, 430074, Wuhan, China

²Shandong Provincial Lunan Geology and Exploration Institute (Shandong Provincial Bureau of Geology and Mineral Resources NO.2 Geological Brigade), 272100, Yanzhou, China

Corresponding author: Huirong Guo (hrguo@cug.edu.cn)

Key Points:

- 22 diffusion coefficient data are obtained at 10-50 MPa and 353.15-433.15 K.
- Diffusion coefficient is used to predict when salt precipitation occurs at a site of Alberta Basin.
- Salt precipitation for CO₂ dry-out was observed in a capillary tube and a micromodel respectively.

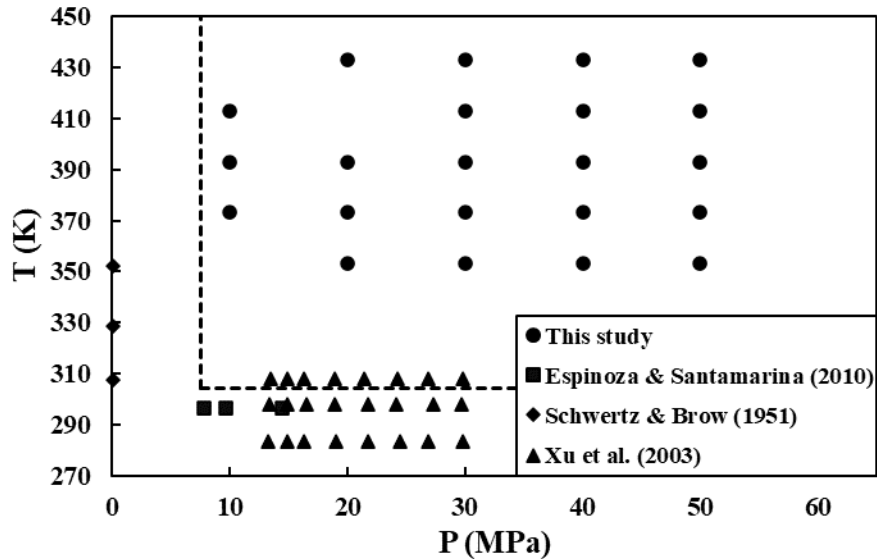
15 **Abstract**

16 CO₂ geological storage is a promising method to dispose excess CO₂ in the atmosphere, and the
17 existence of brine in deep saline aquifer and below oil reservoir may lead to salt precipitation in
18 pore space for dry-out formation. Water diffusion coefficient is helpful to evaluate salt
19 precipitation. However, limited previous data can't satisfy the need of CO₂ geological storage.
20 Raman quantitative spectroscopy is used to observe water diffusion in CO₂ in a high-pressure
21 capillary cell and corresponding diffusion coefficients are obtained at 10-50 MPa and 353.15-
22 433.15 K. Diffusion coefficient is temperature and pressure dependent, and also increases
23 linearly with the reciprocal of CO₂ density. Free volume theory and PC-SAFT EOS are utilized
24 to establish a thermodynamic model for water diffusion in CO₂, and it predicts diffusion
25 coefficient accurately at 10-50 MPa and 353.15-433.15 K. Besides, diffusion coefficient is used
26 to evaluate when salt precipitation occurs and salt precipitation process is observed in a one-
27 dimensional capillary tube and a two-dimensional micromodel respectively.

28 **1 Introduction**

29 CO₂ concentration increases clearly in the atmosphere for huge energy demand (Guyant
30 et al., 2015; Roels et al., 2014), and for now, injecting CO₂ into geological formations is a
31 promising method to mitigate CO₂ emission, including saline aquifer, producing/depleted oil
32 field and coal bed (Bai et al., 2018; Miri et al., 2015; Muller et al., 2009). For saline aquifer and
33 oil field, dissolution is a major mechanism, including CO₂ dissolution in brine and oil (Guo et al.,
34 2016; Han & McPherson, 2009) and when CO₂ contacts brine, CO₂ plume displaces brine and
35 interphase mass transfer exists between CO₂ and brine (Pruess & Müller, 2009) which means dry
36 CO₂ dissolves into water and also dries out water at the same time (Ott et al., 2015). CO₂
37 evaporating water increases brine concentration, and when salt concentration reaching salt
38 solubility, salt precipitation will occur (Muller et al., 2009) which has a obvious effect on CO₂
39 injectivity and storage safety (Gaus, 2010). Generally, salt precipitation near injection wells does
40 impair injectivity (Jeddizahed & Rostami, 2016; Muller et al., 2009) while that near reservoir
41 covers is beneficial for storage safety (Gaus, 2010). Water evaporation rate, in other words,
42 diffusion coefficient in CO₂ is desired for evaluating salt precipitation and CO₂ geological
43 storage.

44 There are limited studies about water diffusion in CO₂ in previous study. Xu et al. (2003)
45 utilized NMR to observe the sample cells to obtain the water diffusion coefficient at 283.15 K,
46 298.15 K and 308.15 K and 13-30 MPa. Espinoza and Santamarina (2010) observed the
47 instantaneous droplet volume and surface area to evaluate the water diffusion coefficient in CO₂
48 at the pressure of 7.8-14.4 MPa and temperature of 296.5±1.5 K. Schwertz and Brow (1951)
49 observed the alteration of liquid level in an isothermal atmosphere of CO₂ and measured the
50 water diffusion coefficient at 1 bar and temperature of 307.45 K, 328.55 K and 352.35 K.
51 According to Fig. 1, most previous experimental data are out of CO₂ supercritical condition
52 which is the major condition for CO₂ in geological storage. These experimental data are not
53 suitable for the reservoir condition of CO₂ geological storage.



54

55 **Figure 1.** Pressure and temperature in previous study and this study (Espinoza & Santamarina,
 56 2010; Schwartz & Brow, 1951; Xu et al., 2003). Dashed line: pressure and temperature of CO₂
 57 supercritical condition.

58 Partly like the previous study (Lu et al., 2013), Raman quantitative is used to obtain water
 59 concentration profile in CO₂ in this study. Differently, there is a steady-state and semi-infinite
 60 diffusion in gas phase, and Fick's first law is suitable to explain the diffusion phenomenon.
 61 According to Fick's First Law, diffusion flux and concentration gradient need to be measured to
 62 calculate diffusion coefficient, and for steady-state diffusion, the flux and concentration gradient
 63 are constant. Water diffusion process is observed at 10-50 MPa and 353.15-433.15 K, and based
 64 on the concentration profiles and water change rate, corresponding diffusion coefficients are
 65 obtained. Based on free volume theory and SAFT EOS, a thermodynamic model for water
 66 diffusion was established and is able to predict water diffusion coefficient accurately at 10-50
 67 MPa and 353.15-433.15 K. With the help of this model, the calculated data is used to predict
 68 when salt precipitation occurs at Alberta Basin site 11. What's more, salt precipitation is
 69 investigated in a one-dimensional capillary tube and two-dimensional micromodel to observe the
 70 salt crystal variation and distribution in porous media.

71

72 2 Materials and Methods

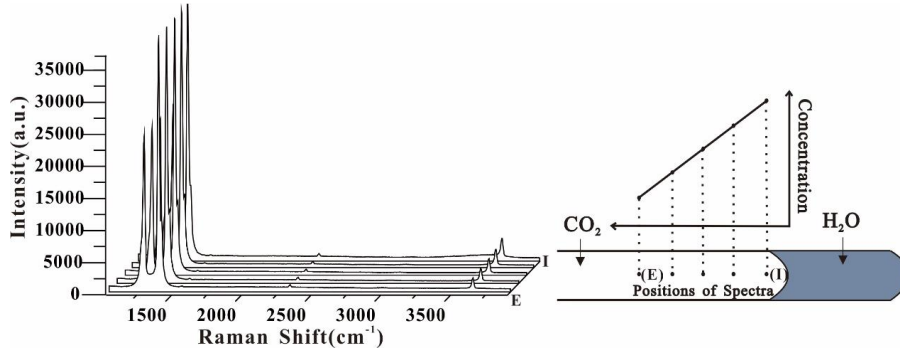
73 2.1 Sample preparation and spectra collection

74 Procedures of sample preparation and material are same as sample loading of (Lu et al.,
 75 2013), but procedures of Raman spectra collection and diffusion coefficient calculation are
 76 different.

77 After sample loading, the sample is kept at the experimental P-T condition for 1-2 days.
 78 When the concentration gradient and interface change rate are constant, there reaches a steady-
 79 state diffusion in the gas phase which accords with Fick's first law. Five certain spots at a
 80 constant distance are chosen to collect Raman spectra to obtain water concentration profile in gas

81 phase (Fig. 2), and at the same time, alteration of interface with time is recorded for calculation
 82 of diffusion flux. Positions for spectra should be changed with the changing interface, for the
 83 purpose of making distance between interface and positions constant.

84 For spectra processing, areas of water peak (3600-3680 cm^{-1}) and CO_2 peak (1150-1500
 85 cm^{-1}) are obtained to calculate the ratio of area PAR [$\text{H}_2\text{O}/(\text{H}_2\text{O}+\text{CO}_2)$]. Raman quantitative
 86 factors have been measured to calculate water concentration in our previous study (Wang et al.,
 87 2018).



88
 89 **Figure 2.** Spectra of diffusion about water in CO_2 . From the interface to the end, the area of
 90 water decreases linearly. It indicates concentration of water in CO_2 decreases linearly, and it
 91 comes to a steady-state diffusion.

92 2.2 Calculation of water diffusion coefficient

93 Fick's first law is

$$94 \quad J = -D \frac{dC}{dl} \quad (1)$$

95 J is diffusion flux; C is concentration of solute; l is distance; D is diffusion coefficient.

96 Diffusion flux means the velocity of water decreasing. Thus:

$$97 \quad \frac{\Delta L \times A}{V_m^L} = D \times \frac{\Delta C}{\Delta l} \times \Delta t \times A \quad (2)$$

98 ΔL is the alteration of water length, m; A is the area of tube section, m^2 ; V_m^L is mole
 99 volume of water, cm^3/mol ; Δt is the alteration of time, s; D is diffusion coefficient, m^2/s ; C is
 100 concentration of water in carbon dioxide, mol/m^3 ; Δl is the alteration of distance in different
 101 observation positions, m.

102 Raman quantitative factors (Wang et al., 2018) and PAR are used to calculate the
 103 concentration of water in CO_2 .

$$104 \quad C = \frac{x_{\text{H}_2\text{O}}}{(1-x_{\text{H}_2\text{O}}) \times V_m^G} \quad (3)$$

105 Then

$$106 \quad \Delta C = C_2 - C_1 = \frac{x_2}{(1-x_2) \times V_m^G} - \frac{x_1}{(1-x_1) \times V_m^G} \quad (4)$$

107 According to Fick's first law, the equation is written as

$$\frac{\Delta L}{\Delta t} = \frac{\frac{x_1}{(1-x_1)} - \frac{x_2}{(1-x_2)}}{\Delta l} \times D \times \frac{V_m^L}{V_m^G} \quad (5)$$

Thus, the concentration gradient in gas phase is:

$$K_1 = \frac{\frac{x_1}{(1-x_1)} - \frac{x_2}{(1-x_2)}}{\Delta l} \quad (6)$$

In the study, the diffusion flux of water is expressed as the variation of interface, which is:

$$K_2 = \frac{\Delta L}{\Delta t} \quad (7)$$

According to (5), (6) and (7), diffusion coefficient is:

$$D = \frac{K_2 V_m^G}{K_1 V_m^L} \quad (8)$$

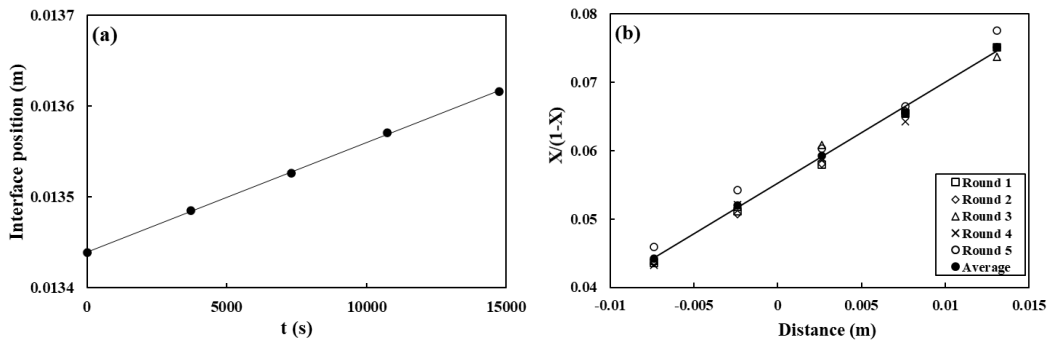
2.3 Observation of salt precipitation

Salt precipitation is observed in a capillary tube as a single pore and a micromodel as a two dimensional porous medium. Load the brine into the capillary tube and micromodel. Evacuate the air and inject into CO₂, and maintain the pressure and temperature using the heating-cooling stage and pressure pump. Observe the salt precipitation process until the all water is evaporated.

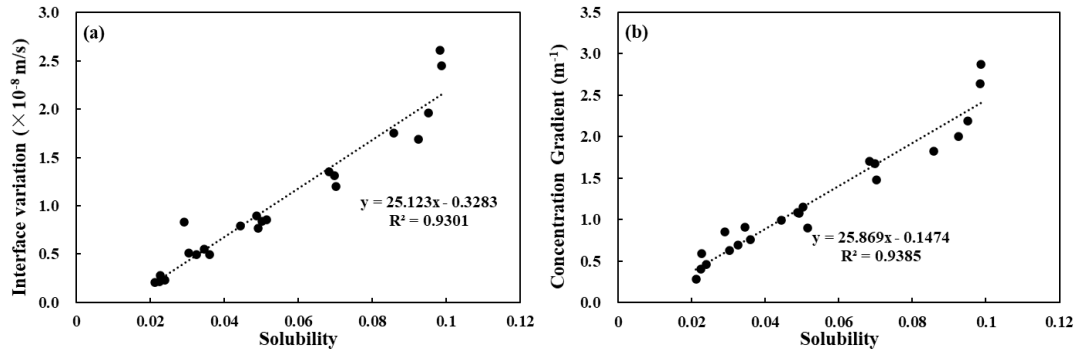
3 Results

3.1 Diffusion observation

In this study, there is a steady-state diffusion for water in CO₂. Because CO₂ concentration in water reaches solubility, no more CO₂ dissolves in water 1-2 days later (Lu et al., 2013), and the variation of water volume is completely caused by water dissolving into CO₂. Interface changes with time linearly which means water volume also decreases with time linearly (Fig. 3a) and diffusion flux is constant. Besides, according to the measured water concentration profiles, concentration decreases linearly with distance away from the interface, and fitted concentration gradient is generally constant for every round (Fig. 3b). Moreover, water concentration gradient in CO₂ and interface change rate are relevant to water solubility in CO₂ (Wang et al., 2018) (Fig. 4). The relationship can be used to calculate concentration gradient and diffusion flux for CO₂ dry-out effect.



135 **Figure 3.** Diffusion observation at 40 MPa, 413.15 K. (a) Interface changes with time; (b) Water
 136 concentration profiles in CO₂.



137
 138 **Figure 4.** (a) The relationship between interface change rate (representing diffusion flux, K_2) and
 139 water solubility in CO₂; (b) The relationship between water concentration gradient in CO₂ (K_1)
 140 and water solubility in CO₂ (Wang et al., 2018).

141 3.2 Calculated diffusion coefficients

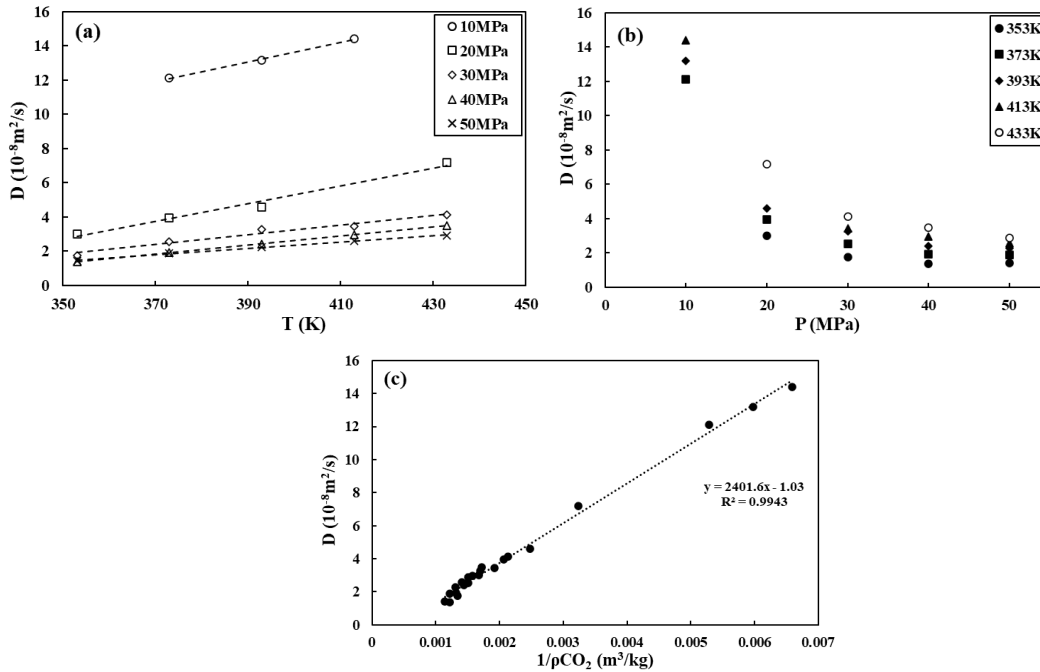
142 By observing the process of the diffusion, water diffusion coefficients in CO₂ were
 143 obtained from 10 to 50 MPa and 353.15 to 433.15 K (Table 1).

144 **Table 1.** Calculated water diffusion coefficient in carbon dioxide ($10^{-8} \text{ m}^2/\text{s}$).

T(K)	10 MPa	20 MPa	30 MPa	40 MPa	50 MPa
353		3.02	1.76	1.37	1.41
373	12.13	3.96	2.55	1.91	1.89
393	13.18	4.60	3.29	2.41	2.26
413	14.41		3.46	2.96	2.60
433		7.18	4.12	3.50	2.90

145 According to calculated results, there's a certain relationship between diffusion
 146 coefficient and temperature. The result indicates that at 10 to 50 MPa and 353.15 to 433.15 K,
 147 the diffusion coefficient increases linearly with temperature at the same pressure and the slope
 148 decreases with increasing pressure (Fig. 5a). Besides, diffusion coefficient decreases obviously
 149 with the increasing pressure at the same temperature (Fig. 5b). At low pressure, pressure affects
 150 diffusion coefficient more than temperature. Effect of pressure can not be neglected which is
 151 different from CO₂ diffusion in water (Lu et al., 2013).

152 Diffusion coefficient is also affected by the density of solvent, and with density
 153 increasing, diffusion coefficient decreases (Yang et al., 2000). Comparing diffusion coefficient
 154 in this study and CO₂ density, there's a linear relationship between diffusion coefficient and the
 155 reciprocal of CO₂ density (Fig. 5c). It is significant to use CO₂ density to calculate diffusion
 156 coefficient in different temperature and pressure. Comparing between calculation from density
 157 and experiment measurement, the average standard deviation is 3.71%.



158

159

160 **Figure 5.** The relationship between thermodynamic parameters and water diffusion coefficient in
 161 CO₂. (a) Temperature; (b) Pressure; (c) CO₂ density.

162

3.3 Comparison with previous study

163

164

165

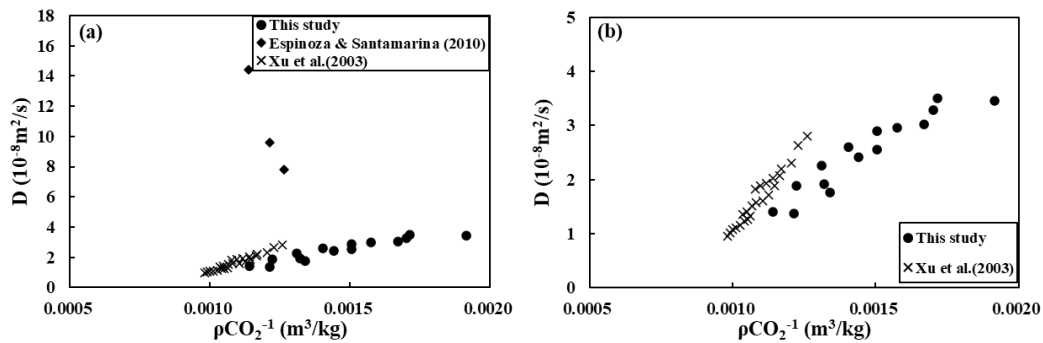
166

167

168

169

Temperature and pressure of previous study (Espinoza & Santamarina, 2010; Xu et al., 2003) are different from those in this study and experimental data can't be compared directly through pressure and temperature. According to the relationship between diffusion coefficient and CO₂ density, it's feasible to replace temperature and pressure with density to compare with previous experimental data. Fig. 6 shows data of Xu et al. (2003) are similar with this study. Comparing the function of diffusion coefficient with density and Xu et al. (2003), the average standard deviation is 8.28%.



170

171 **Figure 6.** Comparison with previous experimental data.

172

3.4 Diffusion model of water in CO₂

173

174

Based on a generalized free-volume model, self-diffusion coefficient can be expressed as (Liu et al., 2002):

$$D_{self} = A_D \sqrt{\frac{kT}{3.14M}} \left(V^* + \frac{V_f}{\gamma} \right) \exp \left(-\frac{\gamma V^*}{V_f} - 2\alpha\varphi \right) \quad (9)$$

D_{self} is the self-diffusion coefficient for fluid; A_D is a constant; k is Boltzmann constant; M is the molar mass; R is the gas constant; V^* is the molar critical free volume; γ is a numerical factor; V_f is the free volume; φ is the mean potential energy.

According the EOS, the compressibility factor (Z) is expressed by attractive (Z^a) and repulsive (Z^r) compressibility. According to the GvdW theory, the Z is expressed as (Liu et al., 2002):

$$Z = V \left(\frac{\partial \ln v_f}{\partial V} \right)_{T,N} - \frac{V}{2kT} \left(\frac{\partial \varphi}{\partial V} \right)_{T,N} = Z^r + Z^a \quad (10)$$

Combining PC-SAFT, Eq. 10 is written as:

$$Z = mV \left(\frac{\partial \ln v_f}{\partial V} \right)_{T,N} - \frac{V}{2kT} \left(\frac{\partial \varphi}{\partial V} \right)_{T,N} = mZ^r + Z^a \quad (11)$$

The free volume theory is correlated with equation of state to evaluate the self-diffusion coefficient of fluid. The PC-SAFT EOS is introduced to correlate the free volume theory. According to the PC-SAFT EOS, the PC-SAFT equation is expressed by the residual Helmholtz energy (Gross & Sadowski, 2001).

$$a^{res} = a^{hs} + a^{chain} + a^{dis} + a^{sas} \quad (12)$$

a^{res} , a^{hs} , a^{chain} , a^{dis} , a^{sas} are the residual, hard-sphere term, chain term, dispersive term and association interaction term hemholtz energy, respectively.

$$a^{res} = -m \ln \left(\frac{V_f}{V} \right) - \frac{\varphi}{2} \quad (13)$$

$$m \ln \left(\frac{V_f}{V} \right) = m \frac{3\eta^2 - 4\eta}{(1-\eta)^2} = -a^{hs} \quad (14)$$

m is the segment parameter in PC-SAFT; η is the reduced density in PC-SAFT (Liu et al., 2002).

Based on the previous study about water and CO₂ self-diffusion coefficients (Kazimierz Krynicki et al., 1978; Robb & Drickamer, 1951; Woolf & Dyo, 1974), modified parameters are listed at Table 2.

Table 2. Parameters for CO₂ and water self-diffusion models.

	CO ₂	Water
α	0.116699	0.138828
A_D	0.843494	117.728

The self-diffusion model is extended to calculate the mutual diffusion coefficient. Mutual diffusion coefficient is mainly determined by solvent property. When water dissolves into CO₂, water molecule replaces CO₂ molecule and can be regarded as CO₂ molecule, and the model of water diffusion in CO₂ is based on CO₂ self-diffusion model. But the activation energy of water is different from that of CO₂. The water diffusion coefficient can be obtained as:

$$D_{12} = A_{D,1} \sqrt{\frac{kT}{3.14M_{12}}} \left(V^* + \frac{V_1^f}{\gamma} \right) \exp \left(-\frac{\gamma V^*}{V_1^f} - \varphi_{12} \right) \quad (15)$$

$$M_{12} = \frac{2M_1M_2}{M_1+M_2} \quad (16)$$

$$\varphi_{12} = \frac{2 \left(-m_1 \ln \left(\frac{V_1^f}{V_1} \right) \alpha_{12} - \beta \alpha_2^{res} \right)}{T^*} \quad (17)$$

$$T^* = \frac{T}{\frac{\varepsilon_{12}}{k}} \quad (18)$$

$$\frac{\varepsilon_{12}}{k} = (1 - a_1) \sqrt{\frac{\varepsilon_1 \varepsilon_2}{k^2}} \quad (19)$$

T^* is the reduced temperature of solvent; φ_{12} is the attractive potential energy; $\varepsilon_1, \varepsilon_2$ are parameters for CO₂ and water respectively from PC-SAFT.

β is dependent on temperature in the following equation:

$$\beta = c_1 + c_2 T^2 \quad (20)$$

Based on experimental data in this study, modified parameters are listed at Table 3.

Table 3. Parameters for model of water diffusion in CO₂.

α_{12}	a_1	c_1	c_2
-0.24687	4.45404	-0.03805	1.28×10^{-6}

Based on the obtained model, the average deviation between calculated data and experimental data is 4.82%, but the average deviation between the model and Xu et al.(2003) is 57.99% (Table 4). This model can predict water diffusion coefficient in CO₂ accurately at 10-50 MPa and 353.15-433.15 K and can't predict that at low pressure and temperature.

Table 4. Relative deviation between the model and experimental data.

This study			Xu et al. (2003)		
P (MPa)	T (K)	Relative Deviation (%)	P (MPa)	T (K)	Relative Deviation (%)
10	373.15	2.65	13.2	283.15	59.86
10	393.15	1.72	14.83	283.15	59.72
10	413.15	1.29	16.26	283.15	59.91
20	353.15	6.69	18.98	283.15	59.24
20	373.15	0.25	21.77	283.15	59.35
20	393.15	9.11	24.49	283.15	59.55
20	433.15	7.85	26.87	283.15	95.86
30	353.15	9.83	29.8	283.15	58.10

30	373.15	0.60	13.33	298.15	57.83
30	393.15	2.97	14.83	298.15	55.63
30	413.15	8.74	16.46	298.15	53.60
30	433.15	3.25	18.91	298.15	53.24
40	353.15	16.55	21.77	298.15	54.80
40	373.15	7.60	24.15	298.15	55.32
40	393.15	4.54	27.28	298.15	54.27
40	413.15	0.70	29.73	298.15	54.32
40	433.15	5.28	13.47	308.15	57.12
50	353.15	0.89	14.9	308.15	56.81
50	373.15	5.59	16.33	308.15	53.26
50	393.15	4.28	18.91	308.15	54.56
50	413.15	3.10	21.43	308.15	53.52
50	433.15	2.53	24.28	308.15	54.47
			26.87	308.15	55.49
			29.8	308.15	56.00

221 3.5 Evaluation of salt precipitation

222 Water diffusion coefficient in CO₂ can be used to calculate the time when precipitation
 223 occurs. Alberta Basin in Canada is a case for CO₂-H₂S saline aquifer storage (Stefan Bachu; John
 224 J. Carroll, 2005). Site 11 is used to apply the experimental data, because the P-T condition of
 225 Site 11 is similar with this study and CO₂ is the major content (82%) of the gas in this site.
 226 Pressure is 24.68 MPa and temperature is 376.15 K in this site, and water diffusion coefficient in
 227 CO₂ is 3.273×10⁻⁸ m²/s. Based on the relationship between solubility (Wang et al., 2018) and

228 concentration gradient, the concentration gradient $\frac{\frac{x_1}{(1-x_1)V_{CO_2}} - \frac{x_2}{(1-x_2)V_{CO_2}}}{\Delta l}$ in this P-T condition is

229 $\frac{0.7197}{76.901 \times 10^{-6}} = 9358.79 \text{ mol/m}^4$. Diffusion flux can be obtained as:

$$230 \quad J = D \frac{\partial C}{\partial l} = 3.273 \times 10^{-8} \times 9358.79 = 3.0631 \times 10^{-4} \text{ mol/(s} \cdot \text{m}^2) \quad (21)$$

231 For simplification, a one-dimensional pore is chosen for evaluation, and the water length
 232 is regards as 2 cm, and salt in brine is NaCl. The salinity is 2.276 mol/kg while the salt solubility
 233 in water is 6.699 mol/kg (Sawamura et al., 2007), and for salt precipitation, water is supposed to
 234 dissolve 66.0%.

235 Based on the calculated diffusion flux,

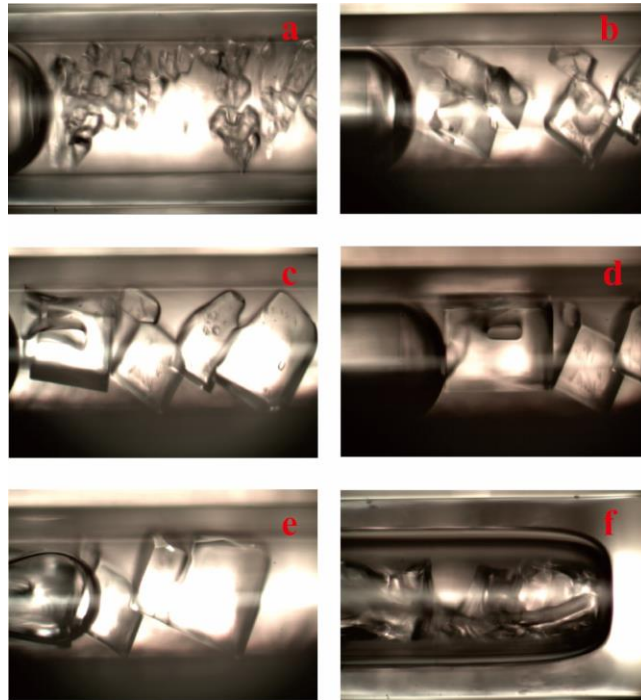
$$236 \quad J \times A \times t = \frac{A \times 2 \times 0.66 \times 0.01}{V_{brine}} \quad (22)$$

$$237 \quad t = \frac{0.0132 / (18.416 \times 10^{-6})}{3.0678 \times 10^{-4}} = 2.3364 \times 10^6 \text{ s} = 27 \text{ day} \quad (23)$$

238 According to the calculation result, salt precipitation will occur 27 days after starting
 239 injecting CO₂ in to saline aquifer. Comparing with the project period, the salt precipitation
 240 occurs too early and will impair CO₂ injectivity.

241 3.6 Observation of salt precipitation in capillary tube

242 For observing the whole process of salt precipitation, small amount of high salinity
 243 solution is used for sample preparation. The length of solution in tube is 3.8 mm and the salinity
 244 is 5 mol/kg, while the experimental pressure and temperature is 20 MPa and 373.15 K. 139 hours
 245 after injecting CO₂, large amount of small crystals appears instantaneously in the solution (Fig.
 246 7a), and crystals grows to be several large cubic crystals with evaporation (Fig. 7b-e). During
 247 growing, crystals are becoming more and more angular and the growing process takes about 43
 248 hours after crystals appear. At the same time, the water is evaporating, and when none liquid
 249 water exists, precipitated crystals are in gas phase, and at the end of tube, crystals are irregular
 250 (Fig. 7f). According to the result, for salt precipitation, gas can only go through the pore between
 251 crystals and pipe well, and the displacement rate is weakened clearly because crystals occupy
 252 much pore space and decreases CO₂-brine interface area.



253
 254 **Figure 7.** Pictures of salt precipitation process.

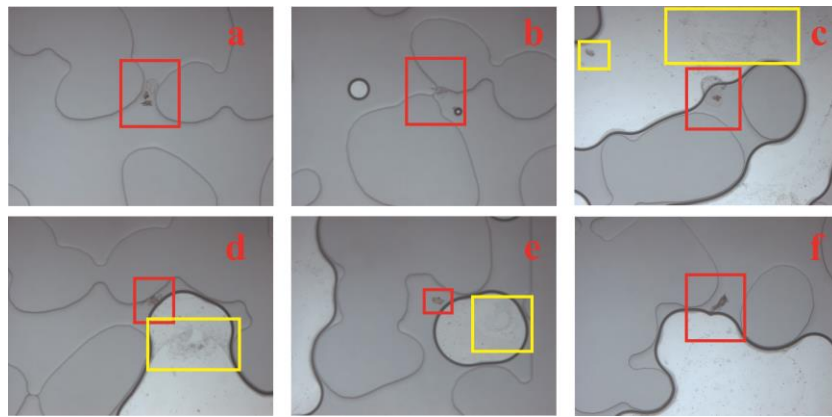
255 3.7 Observation of salt precipitation in micromodel

256 A physical rock type of micromodel is used to observe salt precipitation location in
 257 porous media. The porosity of the micromodel is 0.57. The chip is saturated with 4 mol/kg NaCl
 258 solution and is injected with pure CO₂. The temperature is 294.15±1 K and pressure is 2 MPa.
 259 When injecting CO₂ into the pore space, the displacement phenomenon is different from that in
 260 capillary tube, and at the CO₂-brine mixture zone, there does not exist a specific complete gas-
 261 liquid interface. When CO₂ starts to entry into the brine, CO₂ is surrounded by brine and then,

262 gas saturation becomes larger and brine is surrounded by CO₂ until all brine is dissolved or
 263 displaced.

264 The gas phase is the earliest precipitation zone and salt aggregates form in the gas phase
 265 and near the CO₂ interface. Salt in gas phase is a thin coat on the surface which has little
 266 influence on permeability which has little effect on CO₂ injection. During the first stage, CO₂ is
 267 surrounded by brine and salt precipitation occurs at the whole gas bubble especially at the
 268 interface. With the CO₂ and brine flowing, the salt does not move at all.

269 In the aqueous phase, salt precipitation is more likely to occur at the pore throat (fig.8a,
 270 b) and gas-liquid interface (fig.8d-f) which does weaken permeability and impair CO₂ injectivity.
 271 The salt moves with the flow, and when measuring the permeability after the salt precipitation,
 272 the permeability decreases more than five times mostly due to the accumulation of salt in pore
 273 throat.



274

275 **Figure 8.** Salt precipitation in the micromodel. Red squares are salt in aqueous phase and yellow
 276 means salt in gas phase.

277 5 Conclusions

278 Water diffusion in CO₂ at 10-50 MPa and 353.15-433.15 K is observed by Raman
 279 quantitative spectroscopy and 22 diffusion coefficient data are obtained. Diffusion coefficient
 280 increases with temperature and reciprocal of density linearly and decreases with pressure. Based
 281 on free volume theory and PC-SAFT EOS, a thermodynamic diffusion model for water diffusion
 282 in CO₂ is established and may predict water diffusion coefficient in CO₂ accurately at 10-50 MPa
 283 and 353.15-433.15 K.

284 At the Alberta Basin site 11 injection well, calculated diffusion coefficient is applied to
 285 evaluate when salt precipitation occurs, and it will occur 27 days after CO₂ injection which does
 286 weaken CO₂ injectivity. Salt precipitation observation presents precipitated crystals decrease
 287 pore size dramatically and salt accumulates at the pore throat and gas-liquid interface which
 288 weakens CO₂ mass transfer obviously.

289 Acknowledgments, Samples, and Data

290 This work was supported by the National Sciences Foundation of China (No. 41472218,
 291 41672244) and the Fundamental Research Funds for National Universities, China University of
 292 Geosciences (Wuhan). All the data for this research are included in this submitted paper.

293 **References**

- 294 Bai, B., Wu, H., & Li, X. (2018). Investigation on the relationship between wellhead injection
295 pressure and injection rate for practical injection control in CO₂ geological storage
296 projects. *Geofluids*, 2018. <https://doi.org/10.1155/2018/4927415>
- 297 Espinoza, D. N., & Santamarina, J. C. (2010). Water-CO₂-mineral systems: Interfacial tension,
298 contact angle, and diffusion-Implications to CO₂ geological storage. *Water Resources*
299 *Research*, 46(7). <https://doi.org/10.1029/2009WR008634>
- 300 Gaus, I. (2010). Role and impact of CO₂-rock interactions during CO₂ storage in sedimentary
301 rocks. *International Journal of Greenhouse Gas Control*, 4(1), 73–89.
302 <https://doi.org/10.1016/j.ijggc.2009.09.015>
- 303 Gross, J., & Sadowski, G. (2001). Perturbed-chain SAFT: An equation of state based on a
304 perturbation theory for chain molecules. *Industrial and Engineering Chemistry Research*,
305 40(4), 1244–1260. <https://doi.org/10.1021/ie0003887>
- 306 Guo, H., Huang, Y., Chen, Y., & Zhou, Q. (2016). Quantitative Raman Spectroscopic
307 Measurements of CO₂ Solubility in NaCl Solution from (273.15 to 473.15) K at p =
308 (10.0, 20.0, 30.0, and 40.0) MPa. *Journal of Chemical and Engineering Data*, 61(1), 466–
309 474. <https://doi.org/10.1021/acs.jced.5b00651>
- 310 Guyant, E., Han, W. S., Kim, K. Y., Park, M. H., & Kim, B. Y. (2015). Salt precipitation and
311 CO₂ brine flow distribution under different injection well completions. *International*
312 *Journal of Greenhouse Gas Control*, 37, 299–310.
313 <https://doi.org/10.1016/j.ijggc.2015.03.020>
- 314 Han, W. S., & McPherson, B. J. (2009). Optimizing geologic CO₂ sequestration by injection in
315 deep saline formations below oil reservoirs. *Energy Conversion and Management*,
316 50(10), 2570–2582. <https://doi.org/10.1016/j.enconman.2009.06.008>
- 317 Jeddizahed, J., & Rostami, B. (2016). Experimental investigation of injectivity alteration due to
318 salt precipitation during CO₂ sequestration in saline aquifers. *Advances in Water*
319 *Resources*, 96, 23–33. <https://doi.org/10.1016/j.advwatres.2016.06.014>
- 320 Kazimierz Krynicki, B. Y., Green, C. D., Sawyer, D. W., Krynicki, K., Green, C. D., & Sawyer,
321 D. W. (1978). Pressure and temperature dependence of self-diffusion in water. *Faraday*
322 *Discuss. Chem. Soc.*, 66, 199. <https://doi.org/10.1039/DC9786600199>
- 323 Liu, H., Silva, C. M., & Macedo, E. A. (2002). Generalised free-volume theory for transport
324 properties and new trends about the relationship between free volume and equations of
325 state. *Fluid Phase Equilibria*, 202(1), 89–107. [https://doi.org/10.1016/S0378-](https://doi.org/10.1016/S0378-3812(02)00083-3)
326 [3812\(02\)00083-3](https://doi.org/10.1016/S0378-3812(02)00083-3)
- 327 Lu, W., Guo, H., Chou, I. M., Burruss, R. C., & Li, L. (2013). Determination of diffusion
328 coefficients of carbon dioxide in water between 268 and 473K in a high-pressure
329 capillary optical cell with in situ Raman spectroscopic measurements. *Geochimica et*
330 *Cosmochimica Acta*, 115, 183–204. <https://doi.org/10.1016/j.gca.2013.04.010>
- 331 Miri, R., van Noort, R., Aagaard, P., & Hellevang, H. (2015). New insights on the physics of salt
332 precipitation during injection of CO₂ into saline aquifers. *International Journal of*
333 *Greenhouse Gas Control*, 43, 10–21. <https://doi.org/10.1016/j.ijggc.2015.10.004>

- 334 Muller, N., Qi, R., Mackie, E., Pruess, K., & Blunt, M. J. (2009). CO₂ injection impairment due
335 to halite precipitation. *Energy Procedia*, 1(1), 3507–3514.
336 <https://doi.org/10.1016/j.egypro.2009.02.143>
- 337 Ott, H., Roels, S. M., & de Kloe, K. (2015). Salt precipitation due to supercritical gas injection: I.
338 Capillary-driven flow in unimodal sandstone. *International Journal of Greenhouse Gas*
339 *Control*, 43, 247–255. <https://doi.org/10.1016/j.ijggc.2015.01.005>
- 340 Pruess, K., & Müller, N. (2009). Formation dry-out from CO₂ injection into saline aquifers: 1.
341 effects of solids precipitation and their mitigation. *Water Resources Research*, 45(3), 1–
342 11. <https://doi.org/10.1029/2008WR007101>
- 343 Robb, W. L., & Drickamer, H. G. (1951). Diffusion in CO₂ up to 150-atmospheres pressure. *The*
344 *Journal of Chemical Physics*, 19(12), 1504–1508. <https://doi.org/10.1063/1.1748110>
- 345 Roels, S. M., Ott, H., & Zitha, P. L. J. (2014). μ -CT analysis and numerical simulation of drying
346 effects of CO₂ injection into brine-saturated porous media. *International Journal of*
347 *Greenhouse Gas Control*, 27, 146–154. <https://doi.org/10.1016/j.ijggc.2014.05.010>
- 348 Sawamura, S., Egoshi, N., Setoguchi, Y., & Matsuo, H. (2007). Solubility of sodium chloride in
349 water under high pressure. *Fluid Phase Equilibria*, 254(1–2), 158–162.
350 <https://doi.org/10.1016/j.fluid.2007.03.003>
- 351 Schwertz, F. A., & Brow, J. E. (1951). Diffusivity of water vapor in some common gases. *The*
352 *Journal of Chemical Physics*, 19(5), 640–646. <https://doi.org/10.1063/1.1748306>
- 353 Stefan Bachu; John J. Carroll. (2005). In-situ phase and thermodynamic properties of resident
354 brine and acid gases (CO₂ and H₂S) injected into geological formations in western
355 Canada. *Greenhouse Gas Control Technologies*, 1, 49–451.
- 356 Wang, Z., Zhou, Q., Guo, H., Yang, P., & Lu, W. (2018). Determination of water solubility in
357 supercritical CO₂ from 313.15 to 473.15 K and from 10 to 50 MPa by in-situ quantitative
358 Raman spectroscopy. *Fluid Phase Equilibria*, 476, 170–178.
359 <https://doi.org/10.1016/j.fluid.2018.08.006>
- 360 Woolf, B. Y. L. A., & Dyo, T. (1974). Tracer Diffusion of Tritiated Water (THO) in Ordinary
361 Water (H₂O) und & Pressure, 784–796.
- 362 Xu, B., Nagashima, K., DeSimone, J. M., & Johnson, C. S. (2003). Diffusion of water in liquid
363 and supercritical carbon dioxide: An NMR study. *Journal of Physical Chemistry A*,
364 107(1), 1–3. <https://doi.org/10.1021/jp021943g>
- 365 Yang, X. N., Coelho, L. A. F., & Matthews, M. A. (2000). Near-critical behavior of mutual
366 diffusion coefficients for five solutes in supercritical carbon dioxide. *Industrial and*
367 *Engineering Chemistry Research*, 39(8), 3059–3068. <https://doi.org/10.1021/ie990705d>
- 368
369